ACS APPLIED MATERIALS & INTERFACES

Letter

www.acsami.org

CVD Growth of Graphene on NiTi Alloy for Enhanced Biological Activity

Jinhua Li,[†,‡,§] Gang Wang,[†,⊥,#] Hao Geng,[‡,§] Hongqin Zhu,[‡] Miao Zhang,[⊥] Zengfeng Di,[*,⊥] Xuanyong Liu,[*,‡] Paul K Chu,[∥] and Xi Wang[⊥]

[‡]State Key Laboratory of High Performance Ceramics and Superfine Microstructure, Shanghai Institute of Ceramics, and [⊥]State Key Laboratory of Functional Materials for Informatics, Shanghai Institute of Microsystem and Information Technology, Chinese Academy of Sciences, Shanghai 200050, China

[∥]Department of Physics and Materials Science, City University of Hong Kong, Tat Chee Avenue, Kowloon, Hong Kong China

[§]University of Chinese Academy of Sciences, Beijing 100049, China

[#]School of Physical Science and Technology, Lanzhou University, Lanzhou 730000, China

Supporting Information

ABSTRACT: From the perspective of surface modification of biomaterials, graphene is very promising because of its unique physical and chemical properties. Herein, we report direct in situ fabrication of graphene on nitinol (NiTi) shape memory alloy by chemical vapor deposition (CVD) and investigate both the growth mechanism as well as surface bioactivity of the modified alloy. Growth of the graphene layer is independent of Ni but is rather correlated with the formation of the TiC phase on the surface. Graphene nucleates and grows on this carbide layer during exposure to CH_4. The graphene layer is observed to promote the osteogenesis differentiation of mesenchymal stem cells and surface bioactivity. The use of graphene as a bioactive layer is a viable approach to improving the surface properties of NiTi-based dental and orthopedic implants and components.

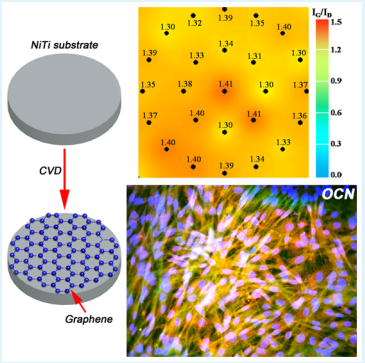

KEYWORDS: *surface and interface, graphene, nitinol, stem cells, bioactivity*

The biocompatibility of NiTi shape memory alloys (SMA) is crucial to biomedical implants and components such as self-expandable cardiovascular stents, stone extraction baskets, catheter guide wires, and orthopedic implants and can be achieved by forming biocompatible phases on the surface and preventing Ni out-diffusion in vivo.[1,2] Since its discovery, graphene has attracted tremendous attention[3,4] in many areas including biomedical engineering, especially as an osteogenic inducer for bone regeneration. In spite of recent investigations on the biocompatibility and osteogenesis activity of graphene,[5,6] exploitation of graphene-based materials in bone regeneration still faces scientific and technical challenges. For instance, the graphene films are free-standing or transferred from other substrates thereby limiting application to hard tissue regeneration. To overcome this hurdle, direct large-area fabrication of graphene on biomedical alloys such as NiTi is a good means to retain the favorable mechanical attributes of the bulk materials while taking advantage of the biocompatibility of graphene.

Graphene can be prepared on Ni[7] as well as other binary alloys such as NiCu,[8] NiAu,[9] and NiMo[10] via a carbon dissolution-segregation mechanism. However, direct growth of graphene on NiTi alloys has seldom been reported, although NiTi alloys with the unique shape memory and superelastic properties are very attractive to biomedical applications. Herein, we report the direct fabrication of graphene on NiTi by chemical vapor deposition (CVD) to promote the osteogenesis differentiation of mesenchymal stem cells and surface bioactivity.

The fabrication process of graphene is summarized in Figure 1a. A circular NiTi disc with a Ni concentration of 50.8 at % and thickness of 1 mm is annealed at different temperature between 950 and 1050 °C in a CVD chamber under Ar and CH_4 (Table 1). The pristine NiTi is prepolished to a shiny surface texture (Figure 1b) and Figure 1c–e show that by controlling the CVD conditions, graphene can be fabricated uniformly on NiTi as a "wormlike" interconnected structure. The influence of the fabrication temperature is explored. At 950 °C, a wormlike texture emerges. The 2D and G peaks typical of graphene appear in conjunction with a defect-related D peak (Figure 1f). When the growth temperature is elevated to 1050 °C, the wormlike texture becomes clearer (Figure 1e) and the graphene crystalline improves as indicated by the attenuated D peak (Figure 1f). To evaluate the uniformity and coverage of graphene layer, we analyzed 25 points on the sample by Raman scattering and the I_G/I_D ratio maps are depicted in Figures 1g–

Received: July 22, 2015
Accepted: August 31, 2015
Published: August 31, 2015

DOI: 10.1021/acsami.5b06639
ACS Appl. Mater. Interfaces 2015, 7, 19876–19881

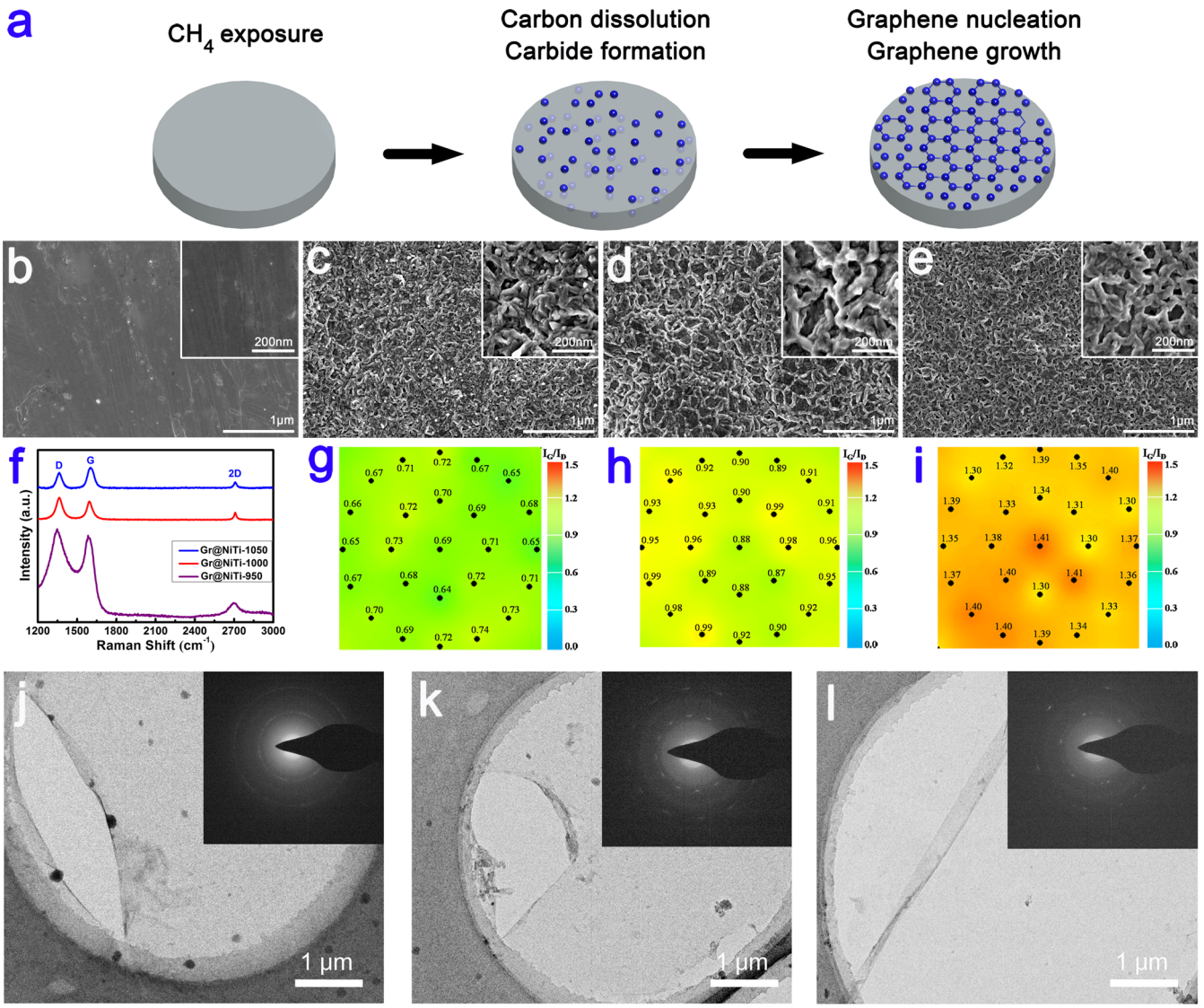

Figure 1. (a) Schematic illustration of the preparation of a large-area graphene layer on NiTi by CVD; surface morphology of the (b) NiTi control and graphene samples prepared at (c) 950, (d) 1000, and (e) 1050 °C; (f) Raman spectra and mappings of the graphene layer grown on NiTi for (g) 950, (h) 1000, and (i) 1050 °C; TEM results of the graphene layer transferred from the NiTi foil for (j) 950, (k) 1000, and (l) 1050 °C.

Table 1. Important Instrumental Conditions in the CVD Process for the Fabrication of Graphene on NiTi Alloy

samples	T (°C)	argon (sccm)	CH_4 (sccm)
Gr@NiTi-950	950	200	20
Gr@NiTi-1000	1000	200	20
Gr@NiTi-1050	1050	200	20

i. With regard to the graphene prepared at 950 °C, the I_G/I_D ratios calculated from the 25 points are very similar varying between 0.64 and 0.74, indicating that the graphene layer is quite uniform on this scale. A higher temperature facilitates nucleation and growth of graphene giving rise to a larger grain size and better crystalline quality (Table S1). As a result, the I_G/I_D ratios increase to 1.30−1.41. The improved crystalline quality is confirmed by selected-area electron diffraction (SAED) showing the transformation of a ring to spot pattern with temperature (Figure 1j−l). The correlation between the fabrication temperature and crystalline quality is well-demonstrated by the properties of intermediate graphene prepared at 1000 °C. The wormlike texture is assumed to stem from graphene in lieu of NiTi because no wormlike texture is observed from NiTi while controlling the gas composition during CVD (Table S1) as shown in Figure S1. Direct large-area fabrication of graphene on NiTi obviates the need for a transferring process, boding well for clinical application to orthopedics and bone regeneration.

To elucidate the mechanism of graphene growth on NiTi, the elemental depth profile, chemical states, and phase composition are investigated by XPS and XRD. As shown in Figure 2a, the NiTi alloy forms a native TiO_2 surface layer upon exposure to air.[2] O_2 reacts with Ti in NiTi to form a thin TiO_2 layer depleted with Ni consistent with theoretical simulation.[11] According to thermodynamics (Supporting Information), during CH_4 exposure, NiTi dealloys to form Ti and Ni phases (NiTi(s) → Ni(s) + Ti(s)). Ti reacts with CH_4 to form TiC due to the higher affinity of titanium to carbon than nickel and the TiO_2 phase is converted to TiC phase, ($CH_4(g) + Ti(s) \rightarrow TiC(s) + 2H_2$;$3CH_4(g) + TiO_2(s) \rightarrow TiC(s) + 6H_2(g) + 2CO(g)$), as shown by the XRD patterns. TiC formation depletes Ni from the surface and "snow ploughs" Ni into the

DOI: 10.1021/acsami.5b06639
ACS Appl. Mater. Interfaces 2015, 7, 19876−19881

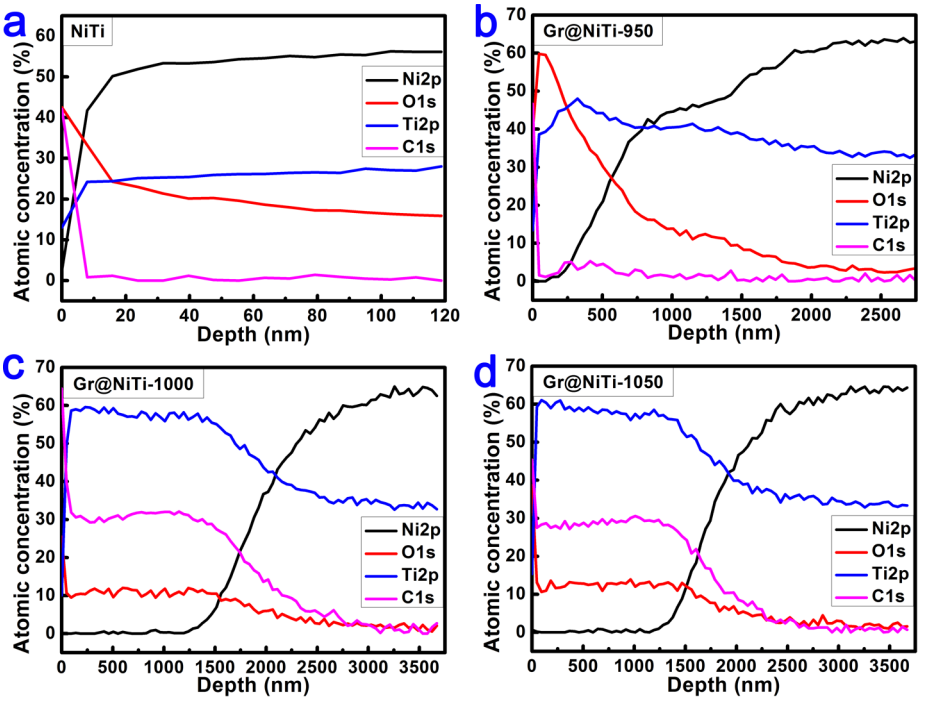

Figure 2. XPS elemental depth profiles of Ni, C, Ti, and O: (a) NiTi, (b) Gr@NiTi-950, (c) Gr@NiTi-1000, and (d) Gr@NiTi-1050.

NiTi substrate underneath the TiC layer (Figure 2b–d). A higher temperature expedites the process and Ni segregation behavior has also been observed from $C_2H_2/O_2/N_2$-implanted NiTi.[12−15] The sp^3-bonded C 1s peak (285.2 eV) gradually disappears and is replaced by the sp^2-bonded C 1s peak from graphene (284.4 eV) (Figure 3a–d). The peak at 281.6 eV is the C 1s peak of TiC.[16] As the fabrication temperature goes up, the Ti 2p doublets of TiO_2 (464.4 and 458.8 eV) shift to 455.1 and 461.1 eV (Figure 3e–h) indicating the formation of a TiC layer on NiTi. As shown in Figure 3i, the untreated NiTi is consisted of austenite and martensite phases with a diffraction peak attributed to rutile TiO_2, keeping stable even at 950 °C (Figure 3j).[17] After CVD, the peak of rutile TiO_2 disappears gradually while the peaks of TiC at 35.9, 60.4, 72.4, and 76.1°, corresponding to the (111), (220), (311), and (222) planes, respectively, emerge (Figure 3j–l).[18] The samples prepared under other conditions (Figures S2–S5) reveal the similar change in the surface states. The XRD and XPS are consistent. The surface TiC layer constitutes a good barrier mitigating Ni out-diffusion (Figure S6).

Depletion of Ni from the surface rules out the possibility of the carbon dissolution-segregation mechanism on Ni[7] and other binary alloys like NiCu,[8] NiAu,[9] and NiMo.[10] The absence of a Ni-carbide phase also excludes graphene growth from Ni-carbide such as Ni_2C.[19] Graphene can be grown on bulk carbides of transition metals by CVD, for instance, bulk TaC and WC.[20,21] Here, the growth of graphene is believed to be closely associated with the TiC layer on NiTi. When NiTi is exposed to CH_4, a layer of TiC forms on the surface. This chemically and thermally stable carbide phase tends to suppress graphene nucleation and the graphene growth competes with surface TiC formation at low temperature mainly due to the fairly high C solubility of Ti and strong interactions between C and Ti atoms.[22] Density functional theory (DFT) investigation discloses that the coexistence of carbide and graphene phases is thermodynamically stable, even in the absence of an additional carbon source such as C_2H_4 and CH_4.[19] Based on these considerations, optimizing the CVD conditions like increasing the annealing temperature and adding extra carbon sources may facilitate graphene nucleation and growth. Indeed, in the investigation of graphene growth on bulk carbide monocrystals such as HfC, TaC, and TiC, epitaxial growth of graphene is observed to depend on the crystalline plane of the transition-metal carbides.[23,24] That is, single-layer graphene can be prepared epitaxially on the (111) surface of these bulk carbides, but not as easily on the (001) surface on which bilayered/multilayered graphene may be formed. In the present work, upon CH_4 exposure and thermal decomposition, a surface TiC phase forms initially on NiTi with the (111), (220), (311), and (222) planes with the (111) plane playing a key role in the epitaxial growth, whereas graphene is not readily formed on the (220) and (311) planes (or bilayered/multilayered graphene is formed). The formation mechanism of graphene on the (111), (220), and (311) planes are different, thus explaining the observed wormlike morphology. During annealing at the optimal temperature of 1050 °C, the composite effects rendered by diffusion and bond formation produce the optimal phase of TiC facilitating graphene growth on NiTi. Single-layer graphene has also been produced on the (111) surface of TiC during reaction with C_2H_4 at 1100 °C.[24] The similar annealing temperature and absence of H_2 during CVD support the proposed mechanism which may be applicable to other TiNi-based shape memory alloys including TiNiMo, TiNiFe, and TiNiNb.

Mesenchymal stem cells (MSCs) are seeded to evaluate the surface biological activity of the graphene-modified NiTi. All the samples support the proliferation of MSCs with a steady upward trend (Figure S7). Figure 4a–d shows the expression levels of osteogenic-related genes (OCN, OPN, BMP-2 and Runx2) revealing significant up-regulation on graphene compared to the NiTi control, especially Gr@NiTi-1050, indicating ongoing osteogenesis of the MSCs and differ-

DOI: 10.1021/acsami.5b06639
ACS Appl. Mater. Interfaces 2015, 7, 19876−19881

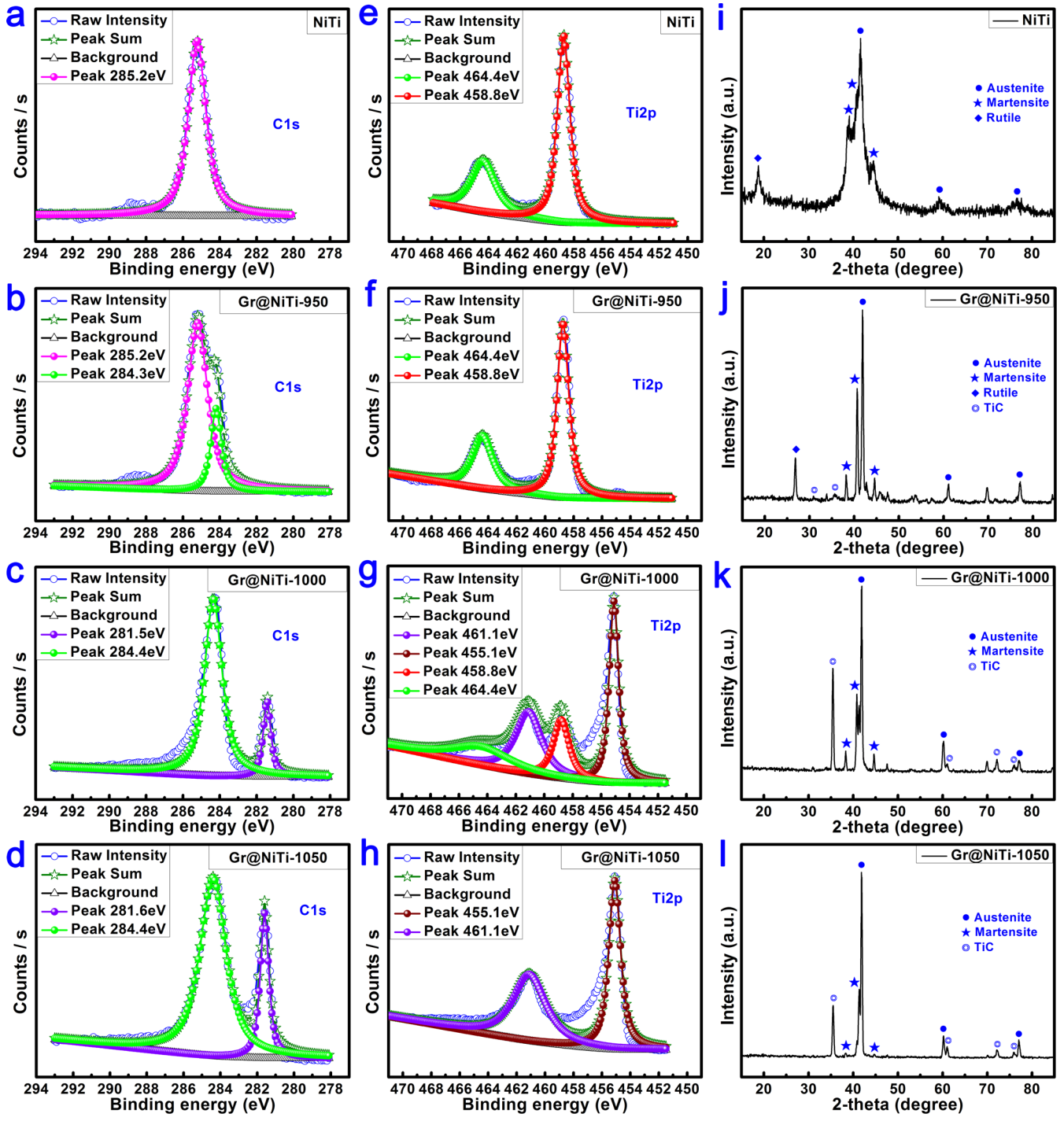

Figure 3. High-resolution XPS spectra of (a–d) C 1s and (e–h) Ti 2p peaks obtained from the surfaces of samples NiTi, Gr@NiTi-950, Gr@NiTi-1000, and Gr@NiTi-1050 together with (i–l) the corresponding surface phase composition and development.

entiation toward osteoblasts. The enhanced OCN expression is confirmed by immunofluorescence at the protein level, as shown in Figure 4e. Meanwhile, ALP staining shows more ALP-positive areas on graphene, especially Gr@NiTi-1050, based on the semiquantification expression (Figure S8). Besides, compared to the sample NiTi, the graphene overlayers can better promote the expression of integrin $\beta 1$ (stained in red) and initial adhesion (actin, stained in green) of the MSCs (Figure 4f), presumably consistent with the enhanced osteogenesis function.[25] Thus, the graphene on NiTi provides an overlayer for its surface bioactivation.[26] It is expected that the osteogenesis inducibility of graphene layer correlates with its defect state. In other words, the higher quality graphene layer on surface has a better promotion effect on osteogenesis than the lower quality one. Having a large area and purely carbon aromatic network, the high-quality graphene layer can provide an open surface for the noncovalent interactions with biomolecules contributed by the $\pi-\pi$ bond. The $\pi-\pi$ stacking can enhance serum protein adsorption, inducer loading, etc., on the surface of graphene layer when culturing MSCs in medium and promote the interactions between cell membrane and graphene layer.[27,28] On the contrary, the defect states of

DOI: 10.1021/acsami.5b06639
ACS Appl. Mater. Interfaces 2015, 7, 19876–19881

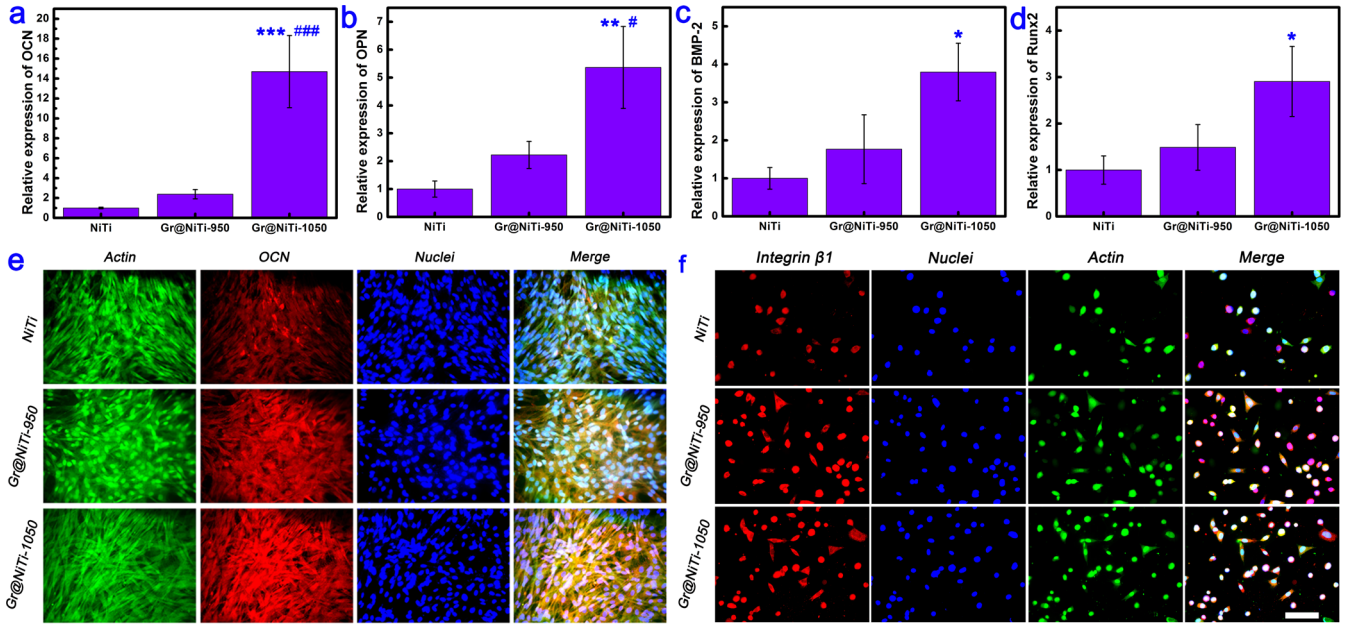

Figure 4. Relative gene expression levels of (a) OCN, (b) OPN, (c) BMP-2, and (d) Runx2 of MSCs cultured on various samples. Notes: $^{*}p < 0.05$, $^{**}p < 0.01$, $^{***}p < 0.001$ versus NiTi; $^{\#}p < 0.05$, $^{\#\#\#}p < 0.001$ versus Gr@NiTi-950. (e) Expression of osteocalcin determined by immunofluorescence assay. Green, actin cytoskeleton; red, osteocalcin positive area; blue, nuclei; yellow, the merged color of green and red. "Merge" represents the merged images of actin, OCN, and nuclei. (f) Expression of integrin β1 detected by immunofluorescence assay. Red color, integrin β1 stained with DyLight 549; Blue color, nuclei stained with DAPI; Green color, actin cytoskeleton stained with FITC-phalloidin. "Merge" represent the merged images of integrin β1, nuclei, and actin. Scale bar, 100 μm.

graphene layer would interrupt the $\pi-\pi$ bond to some extent, which thus results in the low degree of $\pi-\pi$ stacking and electrostatic bonding.[29] For instance, CVD-grown graphene showed a better osteogenesis enhancement than chemically derived graphene oxide, originating from the stronger noncovalent binding ability of the former.[30] Considering the increase of surface hydrophobility (Figure S9) against cell adhesion,[5,26,27] it is inferred that the observed promotion of graphene overlayer on the initial adhesion and osteogenic activity of MSCs mainly originates from the synergistic effect exerted by the wormlike surface topography and the defect-dependent $\pi-\pi$ stacking. Since graphene materials have showing great promise for dental and orthopedic applications, the direct growth of graphene on NiTi reported here enables convenient and viable surface functionalization of NiTi-based alloys to enhance the bioactivity to better meet clinical needs.

In conclusion, a strategy to functionalize NiTi alloy by direct fabrication of graphene in situ by CVD method in order to enhance the bioactivity. The graphene-functionalized NiTi shows better MSCs cytoskeleton development and spontaneous osteogenic differentiation. A higher fabrication temperature improves the crystalline quality of graphene and surface bioactivity. The technique and materials have large potential in dental and orthopedic applications and can be readily extended to other biomedical alloys.

■ ASSOCIATED CONTENT

Supporting Information

The Supporting Information is available free of charge on the ACS Publications website at DOI: 10.1021/acsami.5b06639.

Relevant experimental details pertaining to graphene growth, characterization, cell culture, and evaluation; Tables S1–S3, Scheme S1, and Figures S1–S9 (PDF)

■ AUTHOR INFORMATION

Corresponding Authors

*E-mail: zfdi@mail.sim.ac.cn.

*E-mail: xyliu@mail.sic.ac.cn.

Author Contributions

†J.L. and G.W. contributed equally to this work.

Notes

The authors declare no competing financial interest.

■ ACKNOWLEDGMENTS

Financial support from the National Basic Research Program of China (973 Program, 2012CB933600), National Natural Science Foundation of China (81271704), Shanghai Science and Technology R&D Fund under Grant 14XD1403900, and City University of Hong Kong Strategic Research Grant (SRG) 7004188 are acknowledged.

■ REFERENCES

(1) Liu, X. Y.; Chu, P. K.; Ding, C. X. Surface Modification of Titanium, Titanium Alloys, and Related Materials for Biomedical Applications. *Mater. Sci. Eng., R* **2004**, *47*, 49–121.

(2) Shabalovskaya, S.; Anderegg, J.; Van Humbeeck, J. Critical Overview of Nitinol Surfaces and Their Modifications for Medical Applications. *Acta Biomater.* **2008**, *4*, 447–467.

(3) Geim, A. K. Graphene: Status and Prospects. *Science* **2009**, *324*, 1530–1534.

(4) Kostarelos, K.; Novoselov, K. S. Exploring the Interface of Graphene and Biology. *Science* **2014**, *344*, 261–263.

(5) Luo, Y.; Shen, H.; Fang, Y.; Cao, Y.; Huang, J.; Zhang, M.; Dai, J.; Shi, X.; Zhang, Z. Enhanced Proliferation and Osteogenic Differentiation of Mesenchymal Stem Cells on Graphene Oxide-Incorporated Electrospun Poly(lactic-co-glycolic acid) Nanofibrous Mats. *ACS Appl. Mater. Interfaces* **2015**, *7*, 6331–6339.

(6) Lu, J.; He, Y.-S.; Cheng, C.; Wang, Y.; Qiu, L.; Li, D.; Zou, D. Self-Supporting Graphene Hydrogel Film as an Experimental Platform

DOI: 10.1021/acsami.5b06639
ACS Appl. Mater. Interfaces 2015, 7, 19876–19881

to Evaluate the Potential of Graphene for Bone Regeneration. *Adv. Funct. Mater.* **2013**, *23*, 3494−3502.
(7) Yu, Q.; Lian, J.; Siriponglert, S.; Li, H.; Chen, Y. P.; Pei, S.-S. Graphene Segregated on Ni Surfaces and Transferred to Insulators. *Appl. Phys. Lett.* **2008**, *93*, 113103.
(8) Wan, D.; Lin, T.; Bi, H.; Huang, F.; Xie, X.; Chen, I. W.; Jiang, M. Autonomously Controlled Homogenous Growth of Wafer-Sized High-Quality Graphene via a Smart Janus Substrate. *Adv. Funct. Mater.* **2012**, *22*, 1033−1039.
(9) Weatherup, R. S.; Dlubak, B.; Hofmann, S. Kinetic Control of Catalytic CVD for High-Quality Graphene at Low Temperatures. *ACS Nano* **2012**, *6*, 9996−10003.
(10) Dai, B.; Fu, L.; Zou, Z.; Wang, M.; Xu, H.; Wang, S.; Liu, Z. Rational Design of a Binary Metal Alloy for Chemical Vapour Deposition Growth of Uniform Single-Layer Graphene. *Nat. Commun.* **2011**, *2*, 522.
(11) Nolan, M.; Tofail, S. A. M. Density Functional Theory Simulation of Titanium Migration and Reaction with Oxygen in the Early Stages of Oxidation of Equiatomic NiTi Alloy. *Biomaterials* **2010**, *31*, 3439−3448.
(12) Poon, R. W. Y.; Yeung, K. W. K.; Liu, X. Y.; Chu, P. K.; Chung, C. Y.; Lu, W. W.; Cheung, K. M. C.; Chan, D. Carbon Plasma Immersion Ion Implantation of Nickel-Titanium Shape Memory Alloys. *Biomaterials* **2005**, *26*, 2265−2272.
(13) Yeung, K. W. K.; Poon, R. W. Y.; Liu, X. Y.; Ho, J. P. Y.; Chung, C. Y.; Chu, P. K.; Lu, W. W.; Chan, D.; Cheung, K. M. C. Corrosion Resistance, Surface Mechanical Properties, and Cytocompatibility of Plasma Immersion Ion Implantation-Treated Nickel-Titanium Shape Memory Alloys. *J. Biomed. Mater. Res., Part A* **2005**, *75A*, 256−267.
(14) Yeung, K. W. K.; Poon, R. W. Y.; Liu, X. Y.; Ho, J. P. Y.; Chung, C. Y.; Chu, P. K.; Lu, W. W.; Chan, D.; Cheung, K. M. C. Investigation of Nickel Suppression and Cytocompatibility of Surface-Treated Nickel-Titanium Shape Memory Alloys by Using Plasma Immersion Ion Implantation. *J. Biomed. Mater. Res., Part A* **2005**, *72A*, 238−245.
(15) Poon, R. W. Y.; Ho, J. P. Y.; Liu, X. Y.; Chung, C. Y.; Chu, P. K.; Yeung, K. W. K.; Lu, W. W.; Cheung, K. A. Formation of Titanium Nitride Barrier Layer in Nickel-Titanium Shape Memory Alloys by Nitrogen Plasma Immersion Ion Implantation for Better Corrosion Resistance. *Thin Solid Films* **2005**, *488*, 20−25.
(16) Ihara, H.; Kumashiro, Y.; Itoh, A.; Maeda, K. Aspects of ESCA Spectra of Single Crystals and Thin Films of Titanium Carbide. *Jpn. J. Appl. Phys.* **1973**, *12*, 1462−1463.
(17) Iijima, M.; Ohno, H.; Kawashima, I.; Endo, K.; Brantley, W. A.; Mizoguchi, I. Micro X-ray Diffraction Study of Superelastic Nickel-Titanium Orthodontic Wires at Different Temperatures and Stresses. *Biomaterials* **2002**, *23*, 1769−1774.
(18) Zhang, X.; Huo, K.; Wang, H.; Gao, B.; Fu, J.; Hung, T.-F.; Chu, P. K. Controlled Fabrication of Core−Shell TiO_2/C and TiC/C Nanofibers on Ti Foils and Their Field-Emission Properties. *ACS Appl. Mater. Interfaces* **2012**, *4*, 1037−1042.
(19) Lahiri, J.; Miller, T.; Adamska, L.; Oleynik, I. I.; Batzill, M. Graphene Growth on Ni(111) by Transformation of a Surface Carbide. *Nano Lett.* **2011**, *11*, 518−522.
(20) Aizawa, T.; Souda, R.; Otani, S.; Ishizawa, Y.; Oshima, C. Anomalous Bond of Monolayer Graphite on Transition-Metal Carbide Surfaces. *Phys. Rev. Lett.* **1990**, *64*, 768−771.
(21) Stefan, P. M.; Shek, M. L.; Lindau, I.; Spicer, W. E.; Johansson, L. I.; Herman, F.; Kasowski, R. V.; Brogen, G. Photoemission-Study of WC(0001). *Phys. Rev. B: Condens. Matter Mater. Phys.* **1984**, *29*, 5423−5444.
(22) Seah, C.-M.; Chai, S.-P.; Mohamed, A. R. Mechanisms of Graphene Growth by Chemical Vapour Deposition on Transition Metals. *Carbon* **2014**, *70*, 1−21.
(23) Nagashima, A.; Nuka, K.; Satoh, K.; Itoh, H.; Ichinokawa, T.; Oshima, C.; Otani, S. Electronic Structure of Monolayer Graphite on Some Transition Metal Carbide Surfaces. *Surf. Sci.* **1993**, *287*, 609−613.
(24) Aizawa, T.; Souda, R.; Otani, S.; Ishizawa, Y.; Oshima, C. Bond Softening in Monolayer Graphite Formed on Transition-Metal Carbide Surfaces. *Phys. Rev. B: Condens. Matter Mater. Phys.* **1990**, *42*, 11469−11478.
(25) Treiser, M. D.; Yang, E. H.; Gordonov, S.; Cohen, D. M.; Androulakis, I. P.; Kohn, J.; Chen, C. S.; Moghe, P. V. Cytoskeleton-Based Forecasting of Stem Cell Lineage Fates. *Proc. Natl. Acad. Sci. U. S. A.* **2010**, *107*, 610−615.
(26) Wang, C.-H.; Guo, Z.-S.; Pang, F.; Zhang, L.-Y.; Yan, M.; Yan, J.-H.; Li, K.-W.; Li, X.-J.; Li, Y.; Bi, L.; Han, Y.-S. Effects of Graphene Modification on the Bioactivation of Polyethylene-Terephthalate-Based Artificial Ligaments. *ACS Appl. Mater. Interfaces* **2015**, *7*, 15263−15276.
(27) Jung, H. S.; Lee, T.; Kwon, I. K.; Kim, H. S.; Hahn, S. K.; Lee, C. S. Surface Modification of Multipass Caliber-Rolled Ti Alloy with Dexamethasone-Loaded Graphene for Dental Applications. *ACS Appl. Mater. Interfaces* **2015**, *7*, 9598−9607.
(28) Nayak, T. R.; Andersen, H.; Makam, V. S.; Khaw, C.; Bae, S.; Xu, X.; Ee, P.-L. R.; Ahn, J.-H.; Hong, B. H.; Pastorin, G.; Özyilmaz, B. Graphene for Controlled and Accelerated Osteogenic Differentiation of Human Mesenchymal Stem Cells. *ACS Nano* **2011**, *5*, 4670−4678.
(29) Sydlik, S. A.; Jhunjhunwala, S.; Webber, M. J.; Anderson, D. G.; Langer, R. In Vivo Compatibility of Graphene Oxide with Differing Oxidation States. *ACS Nano* **2015**, *9*, 3866−3874.
(30) Lee, W. C.; Lim, C. H. Y. X.; Shi, H.; Tang, L. A. L.; Wang, Y.; Lim, C. T.; Loh, K. P. Origin of Enhanced Stem Cell Growth and Differentiation on Graphene and Graphene Oxide. *ACS Nano* **2011**, *5*, 7334−7341.

DOI: 10.1021/acsami.5b06639
ACS Appl. Mater. Interfaces 2015, 7, 19876−19881